Loss of MICOS complex integrity and mitochondrial damage, but not TDP-43 mitochondrial localisation, are likely associated with severity of *CHCHD10*-related diseases

Emmanuelle C. Genin[a], Sylvie Bannwarth[a], Françoise Lespinasse[a], Bernardo Ortega-Vila[b], Konstantina Fragaki[a], Kie Itoh[c], Elodie Villa[d], Sandra Lacas-Gervais[e], Manu Jokela[f,g], Mari Auranen[h,i], Emil Ylikallio[h,i], Alessandra Mauri-Crouzet[a], Henna Tyynismaa[i], Anna Vihola[j], Gaelle Augé[a], Charlotte Cochaud[a], Hiromi Sesaki[c], Jean-Ehrland Ricci[d], Bjarne Udd[f,j], Cristofol Vives-Bauza[b], Véronique Paquis-Flucklinger[a,*]

[a] Université Côte d'Azur, Inserm, CNRS, IRCAN, CHU de Nice, France
[b] Research Health Institute of Balearic Islands (IdISB)-Research Unit, Son Espases, University Hospital, Spain
[c] Department of Cell Biology, Johns Hopkins University Scholl of Medicine, Baltimore, MD, USA
[d] Université Côte d'Azur, Inserm, C3M, France
[e] Université Côte d'Azur, Centre Commun de Microscopie Appliquée, France
[f] Neuromuscular Research Center, Tampere University and University Hospital, Tampere, Finland
[g] Department of Clinical Neurosciences, Turku University Hospital, University of Turku, Turku, Finland
[h] Clinical Neurosciences, Neurology, University of Helsinki, Helsinki University Hospital, Helsinki, Finland
[i] Research Programs Unit, Molecular Neurology, University of Helsinki, Helsinki, Finland
[j] Folkhälsan Institute of Genetics, Department of Medical Genetics, Haartman Institute, University of Helsinki, Helsinki, Finland

ARTICLE INFO

ABSTRACT

Following the involvement of *CHCHD10* in FrontoTemporal-Dementia-Amyotrophic Lateral Sclerosis (FTD-ALS) clinical spectrum, a founder mutation (p.Gly66Val) in the same gene was identified in Finnish families with late-onset spinal motor neuronopathy (SMAJ). SMAJ is a slowly progressive form of spinal muscular atrophy with a life expectancy within normal range. In order to understand why the p.Ser59Leu mutation, responsible for severe FTD-ALS, and the p.Gly66Val mutation could lead to different levels of severity, we compared their effects in patient cells. Unlike affected individuals bearing the p.Ser59Leu mutation, patients presenting with SMAJ phenotype have neither mitochondrial myopathy nor mtDNA instability. The expression of $CHCHD10^{S59L}$ mutant allele leads to disassembly of mitochondrial contact site and cristae organizing system (MICOS) with mitochondrial dysfunction and loss of cristae in patient fibroblasts. We also show that G66V fibroblasts do not display the loss of MICOS complex integrity and mitochondrial damage found in S59L cells. However, S59L and G66V fibroblasts show comparable accumulation of phosphorylated mitochondrial TDP-43 suggesting that the severity of phenotype and mitochondrial damage do not depend on mitochondrial TDP-43 localization. The expression of the $CHCHD10^{G66V}$ allele is responsible for mitochondrial network fragmentation and decreased sensitivity towards apoptotic stimuli, but with a less severe effect than that found in cells expressing the $CHCHD10^{S59L}$ allele.

Taken together, our data show that cellular phenotypes associated with p.Ser59Leu and p.Gly66Val mutations in *CHCHD10* are different; loss of MICOS complex integrity and mitochondrial dysfunction, but not TDP-43 mitochondrial localization, being likely essential to develop a severe motor neuron disease.

1. Introduction

Recently, we provided genetic evidence that mitochondrial dysfunction can have a causative effect in motor neuron degeneration (Bannwarth et al., 2014). We reported a large family with a late-onset phenotype including myopathy, motor neuron disease, cognitive decline looking like frontotemporal dementia (FTD) and cerebellar ataxia. In all patients, muscle biopsy showed ragged-red fibers (RRF) and cytochrome *c* oxydase (COX) negative fibers, a hallmark of mitochondrial myopathy, with accumulation of mitochondrial DNA (mtDNA) deletions. Patient fibroblasts presented with respiratory chain deficiency, mitochondrial ultrastructural alterations and fragmentation of the mitochondrial network. We identified a missense mutation (c.176C > T; p.Ser59Leu) in *CHCHD10* that encodes a mitochondrial protein located in the intermembrane space and enriched at cristae junctions (Bannwarth et al., 2014). Mitofilin/MIC60, another protein enriched at mitochondrial cristae junctions, is a central component of mitochondrial contact site and cristae organizing system (MICOS) complex, the integrity of which is required for the formation and/or maintenance of mitochondrial cristae (Friedman et al., 2015). We showed that the expression of the *CHCHD10^{S59L}* mutant allele leads to MICOS complex disassembly and loss of mitochondrial cristae. The abnormalities of the inner membrane found in *CHCHD10* mutant fibroblasts are responsible for nucleoid disorganization, likely explaining the accumulation of mtDNA deleted molecules in patient muscle. Interestingly, the expression of *CHCHD10* mutant alleles inhibits apoptosis by preventing cytochrome *c* release (Genin et al., 2016).

The observation of a frontotemporal dementia-amyotrophic lateral sclerosis (FTD-ALS) phenotype in a mitochondrial disease led us to analyze *CHCHD10* in a cohort of patients with pathologically proven FTD-ALS. Rapidly, our group and others reported *CHCHD10* mutations in patients with FTD-ALS and familial or sporadic pure ALS leading thus secondarily to the identification of a novel gene associated with FTD-ALS clinical spectrum (Chaussenot et al., 2014) (for review see (Cozzolino et al., 2015)). Furthermore, Penttilä and colleagues identified a founder mutation in *CHCHD10* (c.197G > T; p.Gly66Val) in 17 Finnish families with late-onset spinal motor neuronopathy (SMAJ) (Penttilä et al., 2015), and this variant was later reported also in some Finnish patients that clinically had been diagnosed as Charcot-Marie-Tooth disease type 2 (CMT2) (Auranen et al., 2015; Jokela et al., 2016; Penttilä et al., 2017). SMAJ, also called spinal muscular atrophy Jokela type (OMIM #615048), is a relatively benign autosomal dominant form of spinal muscular atrophy (SMA). Symptoms commonly appear after the age of 30–40. The disease is slowly progressive and the patients remain ambulant for several decades after onset of symptoms with a life expectancy within normal range.

A key pathological feature in the vast majority of ALS and FTD patients is the accumulation of cytoplasmic TDP-43 inclusions (Arai et al., 2006; Neumann et al., 2006). Increasing evidence indicates that TDP-43 accumulates in the mitochondria of neurons from subjects with ALS or FTD and induces mitochondrial dysfunction resulting in synaptic damage (Wang et al., 2013, 2016; Woo et al., 2017). However, the pathogenic mechanisms by which mitochondrial TDP-43 leads to mitochondrial dysfunction remain largely unknown. Recent results have tied together the activities of CHCHD10 to TDP-43 cytoplasmic inclusions by showing that the overexpression of *CHCHD10* mutations resulted in mislocalization of TDP-43 in the cytoplasm (Woo et al., 2017). In order to understand why the p.Ser59Leu and p.Gly66Val mutations, both located in the α-hydrophobic helix of the CHCHD10 protein, respectively lead to severe and mild motor neuron disease, we compared their respective effects on mitochondrial functions, TDP-43 metabolism and cell death in human cellular models.

2. Materials and methods

2.1. Patients

Clinical features of the seven patients carrying the heterozygous p.Gly66Val mutation are listed in Supplementary Table 1. Age at onset ranged from 25 to 60 years frequently with painful cramping. All patients presented with a slowly progressive, proximal and distal motor neuronopathy with reduced tendon reflexes. P1, P3, P4 and P5 patients respectively correspond to P5, P10, P9 and P2 individuals in (Penttilä et al., 2015). Blood and tissue samples were obtained after patients had given informed consent.

2.2. mtDNA molecular analysis

Total DNA was extracted using standard phenol chloroform procedure. Southern blot analysis was performed as previously described (Moraes et al., 1989).

2.3. Cell culture

Skin punches were obtained from patients after informed consent. Primary fibroblast cultures were established using standard procedures in RPMI supplemented with 10% Fetal Bovine Serum (FBS), 45 μg/ml uridine and 275 μg/ml sodium pyruvate. Cultures were incubated at 37 °C with 5% CO$_2$. For galactose conditions, medium was replaced 24 h before experiments by glucose-free medium containing 5 mM galactose and 5 mM pyruvate (Bannwarth et al., 2014).

HeLa cells were maintained in DMEM supplemented with penicillin (100 U/ml)/streptomycin (0.1 mg/ml), 10% FBS, at 37 °C in a humidified atmosphere with 5% CO$_2$ in air. For transient transfections, HeLa cells were transfected using Lipofectamine 2000 (Invitrogen) according to the manufacturer's instructions.

2.4. Blue native electrophoresis (BN-PAGE)

Mitochondrial membranes were isolated from 2.5×10^6 cells or from 200 μg of pure mitochondria as described previously (Nijtmans et al., 2002). Cells were solubilized with 3% digitonin (wt/vol) (Sigma-Aldrich) and 0.4% (wt/vol) lauryl maltoside (Sigma-Aldrich). Ten microliters of samples were electrophoresed on a 5–13% gradient polyacrylamide gel as described previously (Nijtmans et al., 2002). Transfer of proteins onto a PVDF membrane (Bio-Rad Laboratories) was carried out overnight at 30 V at 4 °C. For second-dimension gel electrophoresis, cells were solubilized with two rounds of digitonin (3% and 1%, wt/vol). A lane excised from the first dimension native gel was first treated for 30 min with denaturing buffer containing 15 mM β-mercaptoethanol and 1% SDS and then washed in 1% SDS for 1 h. The gel strip was electrophoresed on a tricine-SDS-polyacrylamide gel as described previously (Ballinger et al., 1999).

For supercomplex analysis, enriched mitochondrial fraction was solubilized with 6 g/g digitonin. Thirty μg proteins were loaded to a 4–13% Bis-Tris Native gel. Electrophoresis run at 4 mA during 23 h. Proteins were transferred at 63 mA for 24 h to a PVDF membrane.

2.5. Purification of mitochondria from fibroblasts

High-purity mitochondria were obtained following manufacturer's recommendations (Qproteome Mitochondria Isolation Kit, Qiagen). Briefly, fibroblasts were disrupted with ice-cold Lysis Buffer (10 min, 4 °C). After centrifugation (1000 ×*g*, 10 min, 4 °C), cytosolic proteins were removed, and cell pellet was disrupted with ice-cold Disruption Buffer. Complete cell disruption was performed by using a blunt-ended needle and a seringe. After centrifugation (1000 ×*g*, 10 min, 4 °C), pellet containing nuclei, cell debris and unbroken cells were removed. High-purity mitochondria were obtained following centrifugation

(6000 × *g*, 20 min, 4 °C).

2.6. Western blotting

The concentration of proteins was determined using the Pierce BCA assay kit (Thermo Fisher Scientific). 5–25 μg of total protein extracts or 5–15 μg high-purity mitochondria were separated on acrylamide-SDS gels and transferred to PVDF membranes (Millipore). Specific proteins were detected by using different antibodies listed in Supplementary Table 2. Signals were detected using a chemiluminescence system (Immobilon Western HRP Chemilumiscent substrates, Millipore). ImageJ was used to quantified protein signals.

2.7. RT-PCR analysis

Total RNA was extracted from fibroblast cells by using Trizol reagent (Invitrogen) according to the manufacturer's instructions. The cDNA synthesis was performed using 1 μg of each total RNA sample, transcriptor reverse transcriptase and random hexameric primers (Roche applied science). PCR analysis was performed using hot start Taq polymerase (Qiagen). Primers, corresponding to *BIM, SKAR, STAG2* and *MADD* genes, were previously described (De Conti et al., 2015). PCR products were separated on a 2% agarose gel.

2.8. Electron microscopy

For ultrastructural analysis, cells were fixed in 1.6% glutaraldehyde in 0.1 M phosphate buffer, rinsed in 0.1 M cacodylate buffer, post-fixed for 1 h in 1% osmium tetroxide and 1% potassium ferrocyanide in 0.1 M cacodylate buffer to enhance the staining of membranes. Cells were rinsed in distilled water, dehydrated in alcohols and lastly embedded in epoxy resin. Contrasted ultrathin sections (70 nm) were analysed under a JEOL 1400 transmission electron microscope mounted with a Morada Olympus CCD camera.

2.9. OXPHOS spectrophotometric measurements

Enzymatic spectrophotometric measurements of the OXPHOS respiratory chain complexes and citrate synthase were performed at 37 °C on fibroblasts according to standard procedures (Rustin et al., 1994).

2.10. Polarographic study

Polarographic studies on fibroblasts of intact cell respiration and digitonin (0.004%)-permeabilized cells mitochondrial substrate oxidation were carried out as previously described (Rustin et al., 1994).

2.11. ATP measurement

ATP synthesis was measured in digitonin-permeabilized fibroblasts by using a luciferin–luciferase method with malate plus pyruvate as substrates, as described previously (Vives-Bauza et al., 2007).

2.12. Mitochondrial network analysis

For mitochondrial staining, cells were incubated with MitoTracker red (Invitrogen) as previously described (Bannwarth et al., 2014). Antibodies used are described in Supplementary Table 2.

The images were deconvolved with Huygens Essential Software™ (Scientific Volume Imaging) using a theoretically calculated point spread function (PSF) for each of the dyes. All selected images were iteratively deconvolved with maximum iterations scored 40 and a quality threshold at 0.05. The deconvolved images were used for quantitative mitochondrial network analysis with Huygens Essentiel Software™ with the following standardised set of parameters: threshold = 15% and seed = 10% for each cell types and garbage = 10

for fibroblasts and HeLa cells. The quantitative data were further analysed in Microsoft Excel and GraphPad Prism 5 (GraphPad Software). Mitochondrial network length was quantified for 35 randomly-selected individual cells. Data are represented as mean ± S.E.M. Statistical analyses were performed by Student's unpaired *t*-test using GraphPad Prism 5 (GraphPad Software).

2.13. Immunofluorescence of cultured cells

For immunofluorescence studies, cells were treated as previously described (Genin et al., 2016) and antibodies are described in Supplementary Table 2. To analyze the number of Drp1 puncta, images were first converted to binary images with the default threshold setting by ImageJ. The Drp1 puncta on the mitochondria were selected using colocalization analysis of Drp1 and Tom20 signals (mitochondria) by Imaris software. The puncta number and mitochondrial area were quantified by ImageJ, following the puncta density was calculated by dividing the number of Drp1 puncta on mitochondria by the total mitochondrial area.

2.14. Lentivirus

Lentiviruses were generated as described previously (Kageyama et al., 2011; Kim et al., 2007). Briefly, pHR-SIN-CSGW expressing Drp1$_{K38A}$ or empty vector was co-transduced into HEK293T cells with two other constructs, pHR-CMV8.2ΔR and pCMV-VSVG, using Lipofectamine 2000 (Invitrogen). Two days after transfection, the supernatant of transduced cells containing released viruses was collected. The viruses were quick-frozen in liquid nitrogen and stored at −80 °C.

Fibroblasts from patients were infected along with 8 μg/ml polybrene (Millipore), and with either viral supernatant expressing Drp1$_{K38A}$ or empty vector (as control) for 24 h. Then, the medium was replaced and fibroblasts were cultured in DMEM with 10% FBS and 1% penicillin/streptomycin. Following 8–12 days of culture, fibroblasts were harvested for immunofluorescence and mitochondrial network analysis.

2.15. Cell death measurement

Cells were treated either with 1 μM Staurosporine (Sigma-Aldrich) or with 1 μM Actinomycine D (Sigma-Aldrich) as indicated, re-suspended in 200 μl of buffer (150 mM NaCl, 10 mM HEPES, 5 mM KCl, 1 mM MgCl$_2$, 1.8 mM CaCl$_2$) and incubated with annexin V-FITC (BD Biosciences) for 10 min at RT. A volume of 0.5 μg/ml of DAPI (Molecular Probes) was then added, and samples were analysed immediately by flow cytometry using a MACS-Quant Analyzer (Miltenyi Biotec). Antibodies are listed in Supplementary Table 2.

2.16. DEVDase activity

A total of 20 μg of protein (in triplicate) was incubated with 0.2 mM of Ac-DEVD-AMC in 50 mM HEPES pH 8; 150 mM NaCl; 20 mM ethylenediaminetetraacetic acid ± 1 μM Ac-DEVD-CHO. Caspase activity was determined at 460 nm, and specific activities were expressed in ΔOD per minute and per milligram of protein.

3. Results

3.1. Unlike the p.Ser59Leu mutation, the p.Gly66Val variant is not responsible for mitochondrial myopathy with mtDNA instability

Muscle biopsies available from patients carrying the p.Gly66Val mutation did not show a typical mitochondrial myopathy (Auranen et al., 2015; Jokela et al., 2016; Pasanen et al., 2016; Penttilä et al., 2015, 2017). We analysed the mitochondrial genome in the muscle of 5 patients (P1-P5), from 39 to 82 years (Supplementary Table 1). One

patient only (P1) had a few COX-negative fibers (3%) with no RRF at age 70 years (not shown). We found no accumulation of mtDNA deletions by Southern blot analysis and the small amount of deleted molecules observed in some patients was probably age-related (Fig. 1A). These results confirm that the p.Gly66Val variant is not associated with mitochondrial myopathy and mtDNA instability, unlike what is observed with the p.Ser59Leu mutation (Bannwarth et al., 2014).

3.2. A different phenotype in fibroblasts also, with neither MICOS nor OXPHOS assembly defect in cells from patients bearing the p.Gly66Val mutation

To analyze the effects of the pGly66Val mutation on MICOS assembly and mitochondrial functions, we studied fibroblast cells from 2 other patients (P6 and P7) because no skin biopsy was available from affected individuals previously described (P1-P5) (Supplementary Table 1). Blue Native (BN)-PAGE analysis revealed no impairment of assembly of MICOS and OXPHOS complexes (Fig. 1B). BN-PAGE followed by 2D western blotting showed that the steady-state levels of assembled CHCHD10 in MICOS complex are not affected in patient fibroblasts (Fig. 1C). BN-PAGE analysis also revealed no impairment of OXPHOS supercomplex formation (Fig. 1D). We next examined the abundance of several MICOS and OXPHOS proteins in patient-derived fibroblasts and we found normal levels compared to control fibroblasts (Fig. 1E–F and Supplementary Fig. 1). These results show that, in fibroblasts also, phenotypes associated with p.Ser59Leu and p.Gly66Val

mutations are different.

3.3. No ultrastructural alterations in cells expressing the $CHCHD10^{G66V}$ allele, no respiratory chain deficiency and no defect of ATP production in patient-derived fibroblasts

We performed ultrastructural analysis of patient fibroblasts. Electron microscopy did not reveal marked ultrastructural abnormalities in patient mitochondria, which demonstrated numerous, thin, well-defined cristae running perpendicularly to the mitochondrial longitudinal axis, and with a regular pattern of parallel organization (Fig. 2A–C). The p.Gly66Val mutation was then expressed in HeLa cells. We previously shown that the expression of the $CHCHD10^{S59L}$ allele led to a marked defect of the mitochondrial cristae maintenance characterized by loss and desorganization of cristae morphology (Bannwarth et al., 2014). Contrary to overexpression of the $CHCHD10^{S59L}$ allele, the one of the $CHCHD10^{G66V}$ mutant did not lead to abnormal morphology of mitochondria (Supplementary Fig. 2). Only a few abnormal cristae were observed similar to those found in HeLa cells overexpressing the CHCHD10 wild-type allele.

Spectrophotometric analysis of fibroblasts from P6 and P7 cultivated in glucose medium revealed no respiratory chain deficiency and polarographic analysis showed normal oxygen consumption and mitochondrial substrate oxidation (Table 1A, B). Identical experiments were performed on fibroblasts grown in a glucose-free medium containing galactose as previously described (Rouzier et al., 2012).
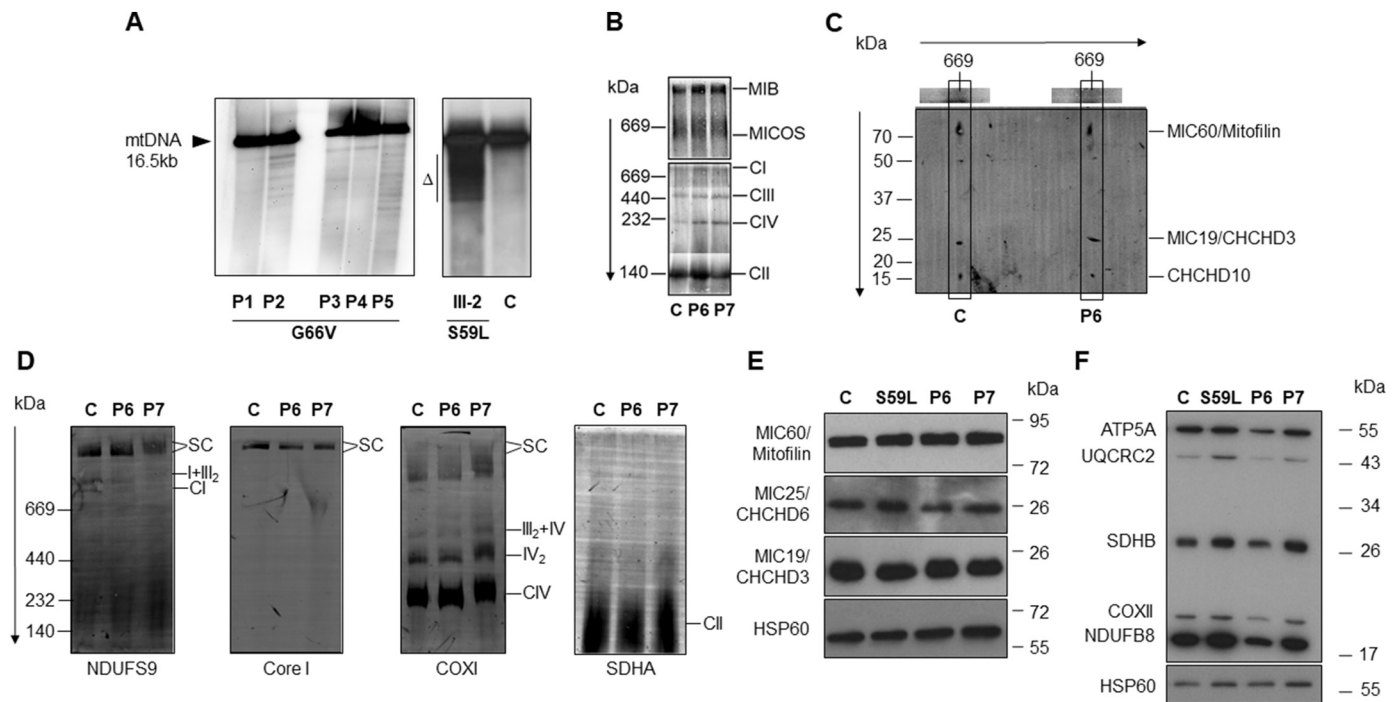

Fig. 1. Analysis of muscle and fibroblasts from patients bearing the p.Gly66Val mutation. A. Southern blot analysis from patient muscle (P1-P5). Comparatively, an accumulation of mtDNA deletions (Δ) was observed in the muscle of a patient (III-2) bearing the p.Ser59Leu mutation (Bannwarth et al., 2014). C: control individual. **B.** BN-PAGE of the MICOS and OXPHOS complexes in control (C) and patient (P6, P7) fibroblasts. Patients P6 and P7 carry the p.Gly66Val mutation. Complexes I to IV (CI-CIV) of OXPHOS were detected with an anti-NDUFS9 antibody (CI), an anti-SDHA antibody (CII), an anti-core I antibody (CIII) and an anti-cytochrome *c* oxidase subunit I antibody (CIV). MICOS and MIB complexes were detected with an antibody anti-MIC60/mitofilin. MIB: Mitochondrial Intermembrane space Bridging complex. **C.** Second dimension of the BN-PAGE showing that the steady-state levels of assembled CHCHD10 in MICOS complex are not affected in patient fibroblasts. **D.** Analysis of OXPHOS supercomplexes in control and patient fibroblasts. BN-PAGE from isolated mitochondria permeabilized with 6 g/g (w/v) of digitonin immunoblotted on PVDF membrane and incubated with the indicated antibodies. SC, supercomplexes I + III2 + IVn. Experiments corresponding to panels B-D, performed with fibroblasts bearing the p.Ser59Leu mutation, are found in Genin et al., 2016. **E.** Representative western blot of MICOS proteins, including mitofilin (MIC60), CHCHD6 (MIC25) and CHCHD3 (MIC19) performed with fibroblast lysates obtained from controls (C1, C2) and patients (P6, P7). Three isoforms of mitofilin (89, 87 and 80kD) exist due to alternative splicing and can be detected by immunoblot analysis. HSP60 was used as a loading control. **F.** Representative western blot of OXPHOS proteins, including ATP5A (CV), UQCRC2 (CIII), SDHB (CII), COXII (CIV) and NDUFB8 (CI) performed with fibroblast lysates obtained from controls (C1, C2) and patients (P6, P7). HSP60 was used as a loading control. Quantitative analysis of blots E and F is found in Supplementary Fig. 1.
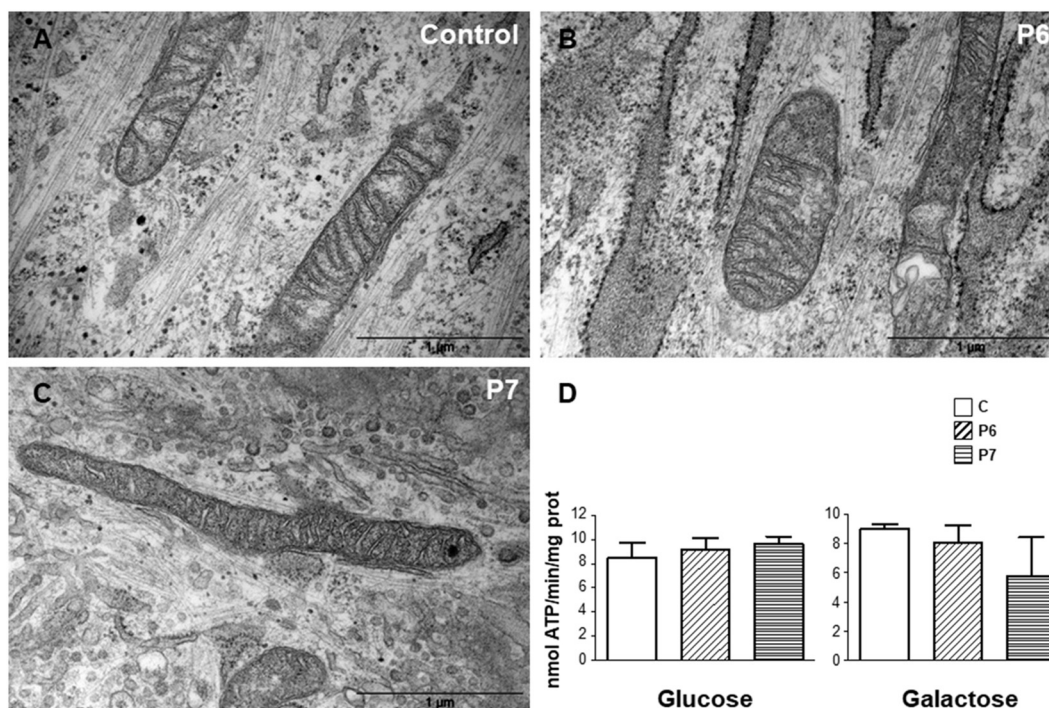
Fig. 2. Ultrastructural analysis and ATP production in patient fibroblasts. Ultrastructural analysis of control (**A**) and patient (P6, **B** and P7, **C**) fibroblasts. Mitochondria with typical normal aspect are found both in control and patient cells. Scale bar = 1 μm. **D.** Measurement of ATP synthesis, by using a luciferin–luciferase method with malate plus pyruvate (30 μM each) as substrates, in digitonin-permeabilized fibroblasts from a control individual (C) and from patients (P6, P7), as indicated. Cells were grown in glucose medium (left panel) or in galactose medium (right panel). Bars represent the mean ± SD of 5 independent experiments.

Galactose is a carbon source that feeds the glycolytic pathway with low efficiency and as such cells are forced to rely predominantly on OX-PHOS for ATP production leading to unmask defects compensated in glucose medium (Robinson et al., 1992). Culture in glucose-free medium only allowed to identify a slight decrease of complex IV/citrate synthase ratio in the fibroblasts of both patients by spectrophotometry while polarography was normal (Table 1C, D). We also found that the pGly66Val mutation does not impair ATP synthesis in patient fibroblasts grown in glucose or in galactose medium (Fig. 2D).

3.4. Comparable accumulation of phosphorylated mitochondrial TDP-43 in fibroblasts from patients bearing the CHCHD10 p.Ser59Leu or p.Gly66Val mutation

A recent study provided a pathological link between CHCHD10 dysfunction and cytoplasmic TDP-43 inclusions (Woo et al., 2017). We therefore examined TDP-43 expression in fibroblasts from patients bearing the p.Ser59Leu or p.Gly66Val mutation (S59L or G66V fibroblasts) or from a control individual. All fibroblasts showed comparable expression of total TDP-43 (Fig. 3A). Interestingly, S59L and G66V fibroblasts displayed a different pattern of mitochondrial TDP-43 than the one found in control cells. Indeed, only phosphorylated TDP-43 was present in the mitochondria of fibroblasts from patients, contrary to control cells which also presented non phosphorylated TDP-43 (Fig.3B–C). In fibroblasts from ALS patients bearing TDP-43 mutations, mitochondrial TDP-43 protein inhibits translation of ND3 and ND6 mRNAs leading to disassembly and dysfunction of complex I (Wang et al., 2016). In S59L and G66V fibroblasts, the mitochondrial location of TDP-43 was not associated with complex I disassembly (Supplementary Fig. 3A, Fig. 1B). However, the expression level of ND3 was decreased both in S59L and G66V fibroblasts, grown in glucose or galactose medium, compared to control cells (Supplementary Fig. 3B). Decreased expression level of ND3 was not sufficient to induce a complex I activity defect in G66V fibroblasts grown in glucose and

galactose medium (Table 1). In S59L cells, the activity of complex I was normal in glucose medium (Bannwarth et al., 2014). In galactose medium, S59L fibroblasts displayed a multiple respiratory chain deficiency which was not limited to complex I, suggesting that mitochondrial TDP-43 toxicity might participate to the respiratory chain defect that we observed (Bannwarth et al., 2014).

In order to also check the general mRNA processing ability of TDP-43 in patient fibroblasts, we performed RT-PCR experiments to analyze splicing efficiency of TDP-43 targets: *BIM, SKAR, STAG2* and *MADD* (De Conti et al., 2015). We found no difference in the patterns of splicing beetwen control and patients cells, suggesting that there is no alteration in the level of different isoform expression (Supplementary Fig. 3C–F).

3.5. Cells expressing the CHCHD10^{G66V} allele display mitochondrial fragmentation

Others and we have shown that the expression of *CHCHD10* mutations, responsible for severe phenotypes (S59L and R15L), in human cells leads to mitochondrial network fragmentation (Bannwarth et al., 2014; Woo et al., 2017) and S59L fibroblasts do not display fusion deficiency (Genin et al., 2016). We compared the mitochondrial network of G66V fibroblasts (P6 and P7) with that obtained from control cells. After staining with Mitotracker and examination by confocal microscopy, control fibroblasts in glucose medium displayed a typical filamentous interconnected network. Patient fibroblasts presented with a fragmentation of the mitochondrial network and less connected mitochondria (Fig. 4A). However, G66V fibroblasts were less fragmented than those harbouring the p.Ser59Leu variant responsible for a severe clinical phenotype (Fig. 4B). The overexpression of the *CHCHD10^{G66V}* allele in HeLa cells confirmed its effect on mitochondrial network fragmentation (Fig. 4C–D).

TDP-43 can form physical complexes with CHCHD10 (Woo et al., 2017). TDP-43 overexpression in transgenic mice induces mitochondrial fragmentation by promoting mitochondrial fission with increased

Table 1
Spectrophotometric and polarographic analysis of the respiratory chain enzyme activities in patient fibroblasts. By spectrophotometry, results are expressed as absolute values for controls or patients, and as activity ratios compared to citrate synthase. Values are expressed in nanomols of substrate per minute per milligram of proteins (lowered values are in bold and highlighted in grey). I-V: complex I-V. CS: citrate synthase. G3P: glycerol 3-phosphate.

A

SPECTROPHOTOMETRIC ANALYSIS ON FIBROBLASTS CULTIVATED IN GLUCOSE MEDIUM						
OXPHOS Enzymatic activities	I	II	III	IV	V	CS
Control values (nmol/min/mg of proteins)	9,0-27,1	18,5-54,0	57,4-176,2	109,9-350,0	22,0-46,2	74,7-161,1
P6	16,8	41,4	112,0	216,0	37,6	109,3
P7	16,6	42,3	138,7	238,7	45,4	138,4

SPECTROPHOTOMETRIC ANALYSIS ON FIBROBLASTS CULTIVATED IN GLUCOSE MEDIUM					
OXPHOS Enzymatic activities ratios	I/CS	II/CS	III/CS	IV/CS	V/CS
Control values	0,09-0,18	0,15-0,53	0,72-2,94	1,16-2,74	0,20-0,57
P6	0,15	0,38	1,02	1,98	0,34
P7	0,12	0,31	1,00	1,72	0,33

B

OXYGRAPHIC ANALYSIS ON FIBROBLASTS CULTIVATED IN GLUCOSE MEDIUM				
Oxygen consumption	Intact cells	Digitonin permeabilized cells		
		Glutamate+Malate	Succinate	G3P
Control values (nmol O2/min/mg of proteins)	5,90-13,80	8,00-16,60	8,00-15,80	4,90-13,50
P6	10,59	12,28	13,94	12,27
P7	10,97	22,14	14,55	8,85

C

SPECTROPHOTOMETRIC ANALYSIS ON FIBROBLASTS CULTIVATED IN GALACTOSE MEDIUM						
OXPHOS Enzymatic activities	I	II	III	IV	V	CS
Control values (nmol/min/mg of proteins)	15,2-20,1	28,2-48,0	88,8-143,0	181,7-315,4	22,7-47,5	124,8-225,0
P6	16,6	35,5	127,9	198,9	47,3	155,7
P7	19,9	33,0	109,4	238,8	43,3	211,3

SPECTROPHOTOMETRIC ANALYSIS ON FIBROBLASTS CULTIVATED IN GALACTOSE MEDIUM					
OXPHOS Enzymatic activities ratios	I/CS	II/CS	III/CS	IV/CS	V/CS
Control values	0,07-0,18	0,15-0,32	0,45-0,93	1,41-1,90	0,13-0,32
P6	0,11	0,23	0,82	**1,28**	0,30
P7	0,09	0,16	0,52	**1,13**	0,20

D

OXYGRAPHIC ANALYSIS ON FIBROBLASTS CULTIVATED IN GALACTOSE MEDIUM				
Oxygen consumption	Intact cells	Digitonin permeabilized cells		
		Glutamate+Malate	Succinate	G3P
Control values (nmol O2/min/mg of proteins)	5,50-18,40	8,10-18,90	8,60-19,40	5,20-17,70
P6	15,66	15,85	19,33	14,73
P7	16,52	15,45	14,55	10,67

levels of Fis1 and Drp1, key components of fission machinery (Wang et al., 2013; Xu et al., 2010). The overexpression of wild-type and *CHCHD10* mutant (S59L and G66V) alleles did not lead to enhanced levels of Fis1 and Drp1 (Fig. 4E). In S59L and G66V fibroblasts, we found no difference regarding Fis1 levels compared to control cells but

Drp1 expression was increased in patient fibroblasts compared to control (Fig. 4F). We therefore studied Drp1 recruitment in patient cells. We used immunofluorescence to visualize Drp1 puncta on mitochondria. Drp1 staining was observed throughout the cytosol, but a portion can be found in punctuate structure in mitochondria. We performed
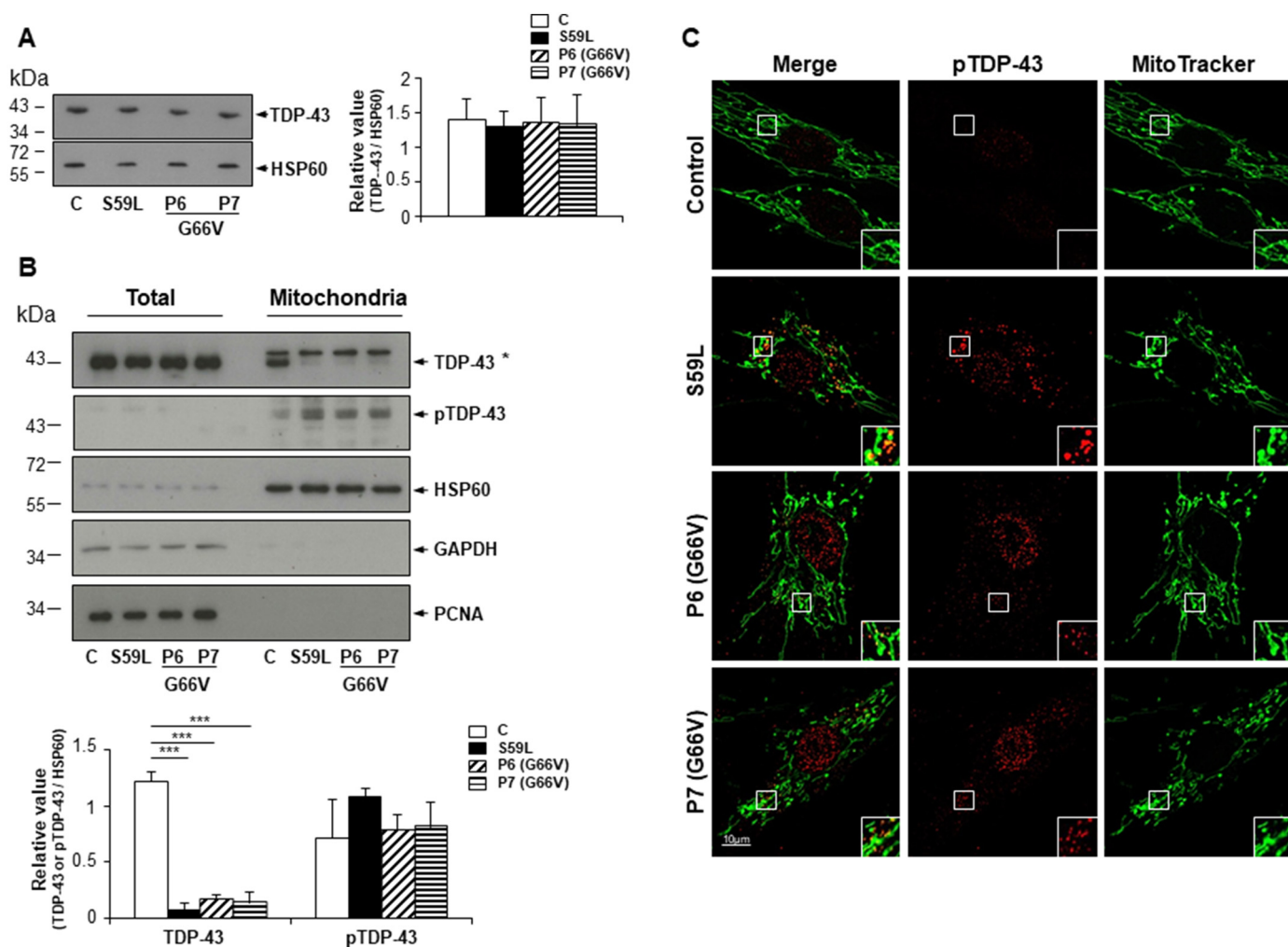
Fig. 3. Accumulation of phosphorylated mitochondrial TDP-43 in S59L and G66V fibroblasts. **A.** Representative western blot and quantification of TDP-43 protein performed with total fibroblast lysates obtained from a control (C) and patients bearing the p.Ser59Leu (S59L) or Gly66Val (P6, P7) mutations. Bars represent the mean ± SD of 3 independent experiments. HSP60 was used as a loading control. **B.** Representative immunoblot of TDP-43 and phosphorylated TDP-43 (pTDP-43) in mitochondria (right panel) and total lysates (left panel) from S59L, G66V (P6, P7) and control fibroblasts. Quantifications of TDP-43 and phosphorylated TDP-43 are performed in mitochondria. TDP-43 antibodies recognize total TDP-43 (including phosphorylated forms) whereas pTDP-43 is specifically directed against phosphorylated TDP-43. After treatment by CIP (Calf Intestinal Phosphatase), probing with pTDP-43 Ab does not allow to reveal any band, thus confirming the specificity of the Ab (not shown). Five micrograms were loaded for mitochondria extracts and total lysates. Bars represent the mean ± SD of 3 independent experiments. Differences between the control and patient fibroblasts were analysed by two-way ANOVA: extremely significant (***$P < 0.001$). HSP60 was used as a loading control. GAPDH and PCNA were used as controls for mitochondrial fraction purity. **C.** Representative images, at confocal microscopy after Huygens deconvolution (Huygens Essential Software™), using Mitotracker and an anti-phosphorylated TDP-43 antibody (pTDP-43), showing partial localization of pTDP-43 in mitochondria of patient cells (overlay in yellow). Enlarged details of the area are indicated. Scale bar: 10 μm. (For interpretation of the references to colour in this figure legend, the reader is referred to the web version of this article.)

image analysis and quantified the density of Drp1 puncta on mitochondria by dividing the number of puncta by the total mitochondrial area (Fig. 5A–B). The density of mitochondrial Drp1 puncta was similar in G66V and control cells. We also analysed S59L fibroblasts and found no difference compared with control cells (Fig. 5A–B). These data suggest that *CHCHD10* mutations have no impact on Drp1 recruitment into patient fibroblasts.

Last, we expressed a dominant negative mutant of the fission protein Drp1 (Drp1$_{K38A}$) (Smirnova et al., 1998) in S59L, G66V and control fibroblasts and found that control and patient cells similarly elongate mitochondria confirming that fusion process is not impaired by the expression of *CHCHD10* mutations (Fig. 5C–D).

3.6. Resistance to apoptosis in cells expressing the CHCHD10^{G66V} allele

We have previously shown that the expression of the *CHCHD10*^{S59L} mutant allele inhibits apoptosis by preventing cytochrome *c* release

(Genin et al., 2016). In order to determine whether the p.Gly66Val mutation leads or not to resistance to apoptosis, we analysed caspase activity in patient fibroblasts. Cells were treated with 1 μM staurosporine (STS) for 6 or 8 h, and caspase activation was determined by DEVDase activity measurement (Fig. 6A). Patient-derived fibroblasts were significantly less sensitive to staurosporine-induced apoptosis compared with control cells. However, they were significantly more sensitive than those bearing the p.Ser59Leu variant, responsible for a severe clinical phenotype. HeLa cells expressing the *CHCHD10*^{G66V} mutant form were also less sensitive to apoptotic cell death than those overexpressing the wild-type CHCHD10 protein (Fig. 6B–D), as observed by the decrease in cleaved caspase 3, the decrease in SMAC degradation (that is a readout of mitochondrial outer membrane permeabilization) and of caspase activity. Taken together our experimental data indicate that expression of the *CHCHD10*^{G66V} allele is able to decrease the sensitivity of the cells towards apoptotic stimuli.
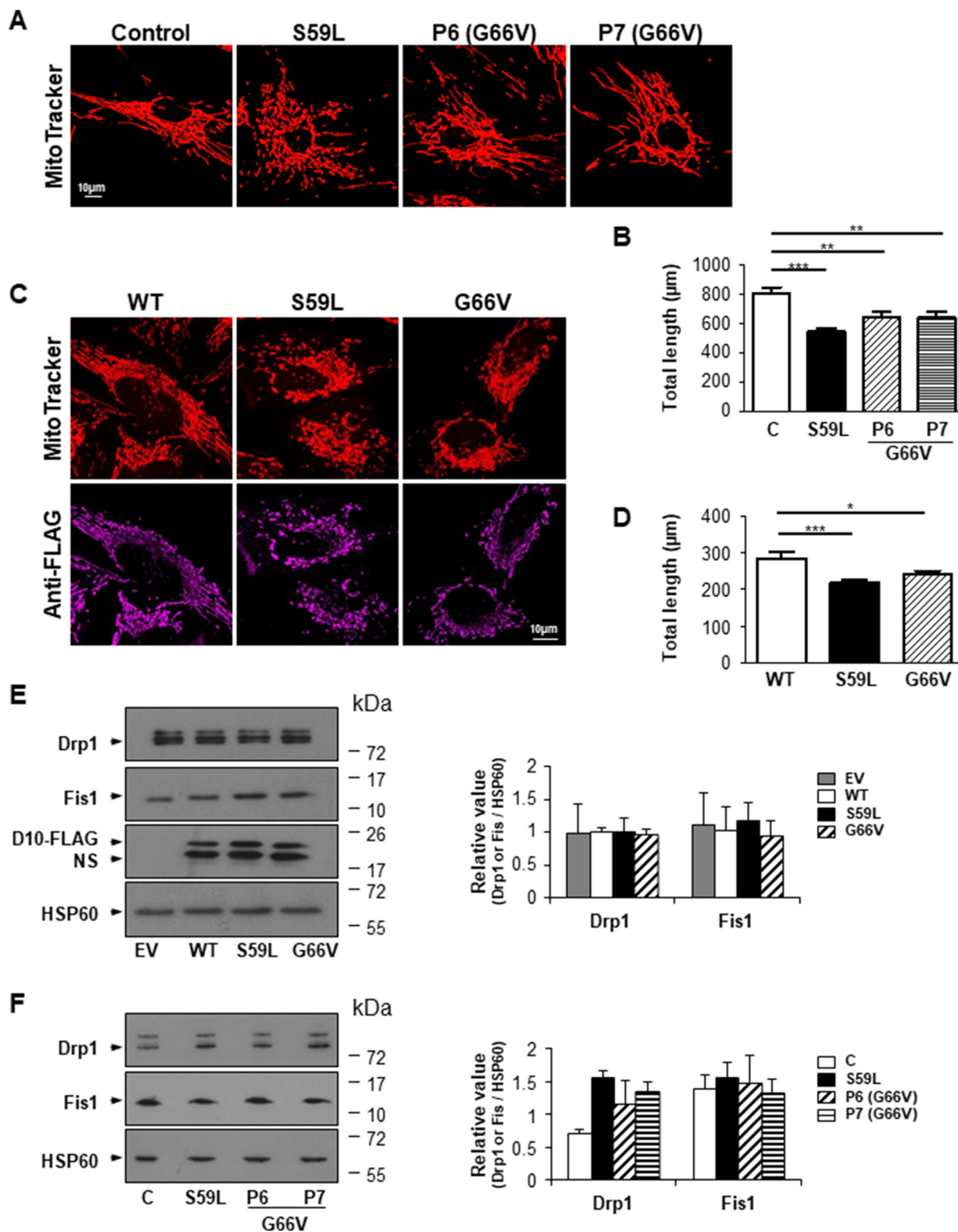
(caption on next page)

4. Discussion

Over the past years, numerous data provided clear molecular evidence that ALS and FTD represent a clinicopathological spectrum of diseases (DeJesus-Hernandez et al., 2011; Janssens and Van Broeckhoven, 2013; Renton et al., 2011; Weishaupt et al., 2016). In addition to overlapping clinical symptoms, the common pathological hallmark found in most ALS and FTD patients is the accumulation of TAR DNA-binding protein 43 (TDP-43) inclusions (Arai et al., 2006; Neumann et al., 2006). TDP-43 plays a major role in the regulation of RNA metabolism and is mainly localized in the nucleus in normal conditions (Buratti et al., 2001). In patient neurons, TDP-43 is depleted from the nucleus and accumulates within cytoplasmic ubiquitinated inclusions. Mutations in *TARDBP*, which encodes TDP-43, are

Fig. 4. Analysis of mitochondrial network and fission proteins in patient fibroblasts. **A.** Control, S59L and G66V (P6, P7) fibroblasts were analysed by confocal microscopy using MitoTracker Red. **B.** Mitochondrial phenotypes shown in A were quantified for 35 randomly-selected individual cells per each studied fibroblast cell line from three independent experiments. The data obtained were used to calculate the total length of the mitochondrial network per cell. Bars represent the mean ± SEM. Differences between the control and patient fibroblasts were analysed by one-way ANOVA: very significant (**$0.01 > P > 0.001$) or extremely significant (***$P < 0.001$). **C.** Analysis of MitoTracker Red staining and FLAG (purple) immunolabelling by fluorescence microscopy in HeLa cells transfected with either wild-type CHCHD10-Flag (WT) or mutant CHCHD10-Flag (S59L or G66V). **D.** Quantification of mitochondrial phenotypes shown in C. Thirty-five randomly-selected individual cells per each transfection were analysed from three independent experiments. The data obtained were used to calculate the total length of the mitochondrial network per cell. Bars represent the mean ± SEM. Differences between the WT CHCHD10-Flag and mutant CHCHD10-Flag (S59 L or G66 V) were analysed by one-way ANOVA: significant (*$0.05 > P > 0.01$) or extremely significant (***$P < 0.001$). **E.** Representative western blot and quantification (from 3 independent experiments) of Drp1 and Fis1 proteins performed with lysates from HeLa cells transfected with empty vector (EV), wild-type CHCHD10-Flag (WT) or mutant CHCHD10-Flag (S59L or G66V). The lower band of Drp1 is the major form (699 amino acids), the upper bands correspond to splicing variants of Drp1. Values are mean ± SD. NS: non specific. **F.** Representative western blot and quantification (from 3 independent experiments) of Drp1 and Fis1 proteins performed with lysates from control (C) and patients fibroblasts. Values are mean ± SD. (For interpretation of the references to colour in this figure legend, the reader is referred to the web version of this article.)

associated with familial and sporadic ALS but TDP-43 inclusions are observed in ALS, FTD and several other neurodegenerative diseases without *TARDBP* mutations (Chanson et al., 2010; Josephs et al., 2015; Kabashi et al., 2008; Sreedharan et al., 2008). It is still unknown whether TDP-43 pathology is caused by nuclear depletion, cytoplasmic accumulation of TDP-43, or both. However, recent studies suggest that the neuronal toxicity of TDP-43 seems, at least in part, due to its mitochondrial localization (Wang et al., 2016). In spinal cord and cortical tissues of ALS or FTD patients, there is a higher expression of TDP-43 in mitochondria than in those from controls (Wang et al., 2016). Fibroblasts from ALS patients bearing *TARDBP* mutations show higher levels of mitochondrial TDP-43 than control cells and overexpression of both wild-type and mutant TDP-43 impairs the expression of complex I ND3 and ND6 subunits and causes complex I disassembly (Wang et al., 2016). Transgenic mouse model expressing the disease-causing human TDP-43 M337V mutant (TDP-43^{M337V} mice) show increased levels of TDP-43 in mitochondria, associated with mitochondrial dysfunction and neuronal loss; the mouse phenotype being reversed by inhibiting the mitochondrial localization of TDP-43 (Wang et al., 2017).

Among all factors involved in ALS pathogenesis, mitochondrial dysfunction has always been recognized as a major player because abnormal mitochondrial structure, respiratory chain deficiency, increased oxidative stress or apoptosis dysfunction have been found in ALS patients and models (Cozzolino et al., 2015). However, whether mitochondria have a causative role in ALS has always been debated. The involvement of *CHCHD10* in ALS-FTD clinical spectrum provided the genetic proof that mitochondrial dysfunction can have a causative effect in motor neuron degeneration (Bannwarth et al., 2014). A recent work showed that CHCHD10 interacts with TDP-43 (Woo et al., 2017). Overexpression of *CHCHD10* mutations (S59L and R15L) causing ALS-FTD disease induced cytoplasmic TDP-43 accumulation, which often co-localized with mitochondria, associated with mitochondrial and synaptic damage. Interestingly, the p.Gly66Val *CHCHD10* mutation is responsible for a less severe motor neuron disease from that associated with the p.Ser59Leu mutation despite their proximity within the N-terminal hydrophobic helix of the protein. Here, we show that G66V and S59L fibroblasts display comparable accumulation of mitochondrial TDP-43. In TDP-43 pathology, TDP-43 is hyperphosphorylated and N-terminally truncated (Arai et al., 2006; Neumann et al., 2006) and the TDP-43 phosphorylated form only was present in the mitochondria of both G66V and S59L fibroblasts. However, G66V fibroblasts do not exhibit respiratory chain deficiency, defect in ATP production, abnormal mitochondrial cristae morphology and MICOS assembly defect, while all of these mitochondrial damage is present in S59L fibroblasts. Our results show that, in the absence of overexpression, mitochondrial accumulation of phosphorylated TDP-43 is not sufficient to induce major mitochondrial damage in *CHCHD10* mutant fibroblasts.

Since mutations in genes encoding mitochondrial fusion proteins like Mfn2 or OPA1, which result in mitochondrial fragmentation, cause neuropathies, it has been hypothesized that mitochondrial

fragmentation may contribute to neurodegenerative disorders (Alexander et al., 2000; Züchner et al., 2004). There is growing evidence suggesting that proteins encoded by mutant alleles that cause Huntington disease or Parkinson disease interact with fission/fusion GTPAses (Knott and Bossy-Wetzel, 2008) and it has been shown that TDP-43 reduces mitochondrial length by promoting mitochondrial fission (Wang et al., 2013). The expression of the *CHCHD10^{S59L}* allele leads to mitochondrial fragmentation, without defect of mitochondrial fusion (Bannwarth et al., 2014; Woo et al., 2017). Our data demonstrate that the p.Gly66Val mutation has the same effect even if this effect is significantly less pronounced than that of the p.Ser59Leu mutation, both in patient fibroblasts and in HeLa cells overexpressing *CHCHD10* mutants. However, we cannot conclude that *CHCHD10* mutations promote mitochondrial fission because patient cells do not display increased levels of Fis1 and despite an increase of Drp1 expression in S59L and G66V fibroblasts, its recruitment is similar to the one found in control fibroblasts. Furthermore, Fis1 and Drp1 levels are not increased by overexpression of *CHCHD10* mutants in HeLa cells. Fragmentation of the mitochondrial network may have other causes than a defect in mitochondrial dynamics and may result, at least in part, from Drp1 activation by reduced levels of phosphatidic acid in the mitochondrial outer membrane. Phosphatidic acid functions as an inhibitor lipid for mitochondrial division (Adachi et al., 2016). Since MICOS is involved in phospholipid biogenesis and transport, the patients may have altered membrane phospholipid composition leading to network fragmentation without increased levels of fission proteins. Taken together, our results suggest that the mitochondrial fragmentation observed in fibroblasts from patients bearing *CHCHD10* mutations is not secondary to a dysregulation of fusion/fission mechanisms.

We previously showed that the expression of wild-type CHCHD10 does not protect HeLa cells from apoptosis induced by actinomycin D (Genin et al., 2016). Surprisingly, the expression of the *CHCHD10^{S59L}* allele led to a reduction in cell death and S59L fibroblasts were significantly less sensitive to staurosporine-induced apoptosis compared with control cells (Genin et al., 2016). We show that the p.Gly66Val mutation also reduces the sensitivity to actinomycin D-induced death, albeit to a lesser extend that in S59L cells. Our results also confirm the surprising anti-apoptotic tendency found in fibroblasts from patients bearing *CHCHD10* mutations leading to motor neuron disease. The recent study describing the functional link between CHCHD10 and TDP-43 showed that overexpression of wild-type CHCHD10 protected HT22 cells from TDP-43 induced apoptosis, whereas R15L and S59L mutations synergized with the pro-apoptotic effect of TDP-43 (Woo et al., 2017). We agree with the authors that this potential discrepancy might be explained by the use of overexpressed proteins in different cellular models and of TDP-43 as a specific stressor. Our data show that, in absence of overexpression and despite an accumulation of mitochondrial phosphorylated TDP-43, S59L and G66V fibroblasts are significantly less sensitive to staurosporine-induced apoptosis compared with control cells.

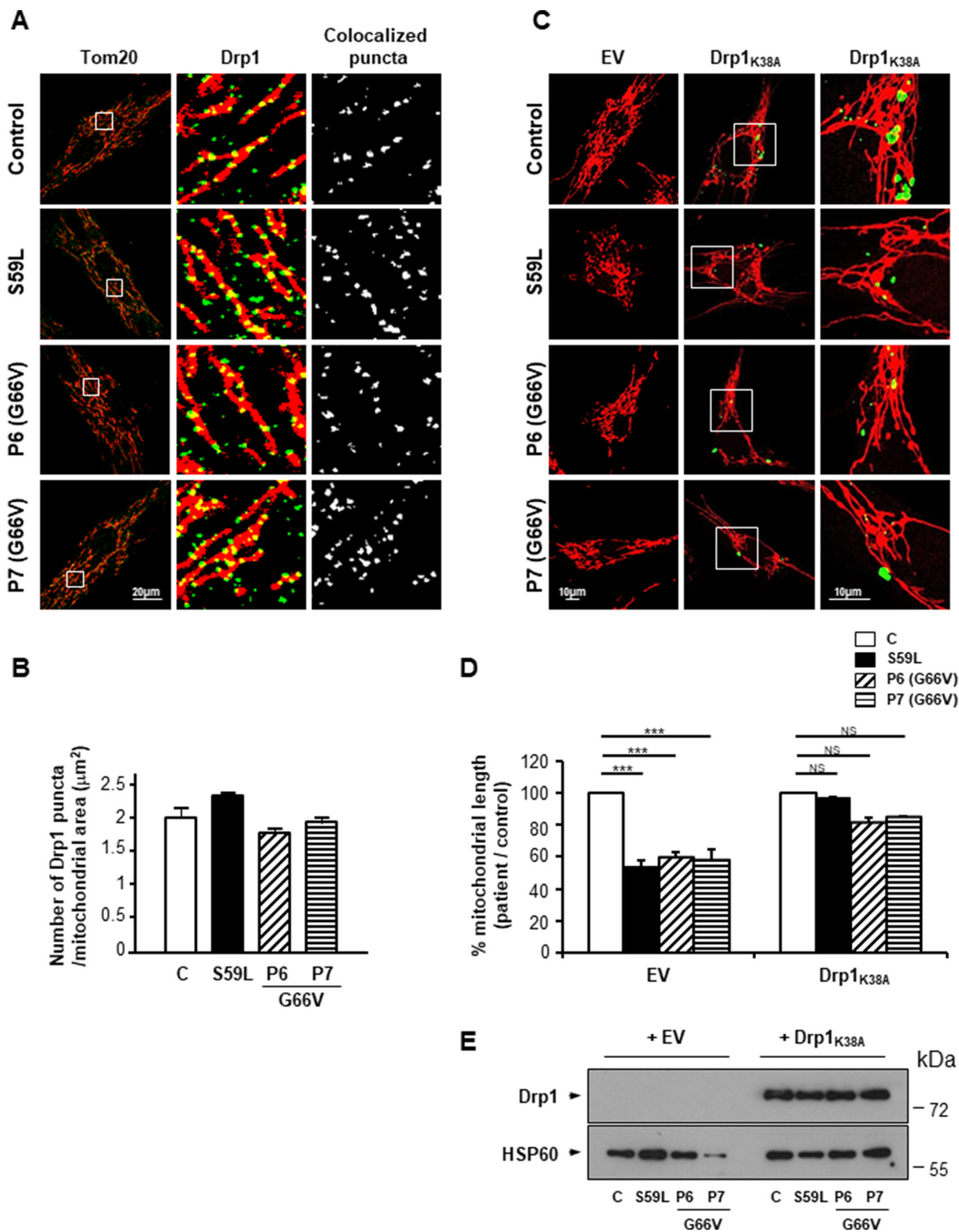Woo and colleagues reported that the effects of the S59L mutation

Fig. 5. Analysis of mitochondrial dynamics in patient fibroblasts. A. Control and patient cells were subjected to immunofluorescence with antibodies to Drp1 (green) and Tom20 (mitochondria, red). Converted binary images are shown. Drp1 puncta on mitochondria were defined using colocalization analysis of Drp1 and Tom20 signals. Scale bar: 20 μm. **B.** The Drp1 puncta numbers on the mitochondria were quantified. Values are mean ± SEM ($n = 10$ cells). **C.** Control and patient cells were infected with lentiviruses carrying the empty vector (EV) or a dominant negative Drp1$_{K38A}$. Cells were subjected to MitoTracker staining (red) and Drp1 immunolabelling (green). The expression of Drp1$_{K38A}$ blocked mitochondrial division and elongated mitochondrial tubules in the control and patient cells. Boxed regions show magnified images. Scale bar: 10 μm. **D.** Quantification of the images shown in C for 25 randomly-selected individual cells per each studied fibroblast cell line (from 2 independent experiments). Values are mean ± SEM. Differences between the control and patient fibroblasts were analysed by one-way ANOVA: extremely significant (***$P < 0.001$). NS: non significant. **E.** Western blot on control and patient fibroblasts, infected with lentiviruses carrying the empty vector (+EV) or a dominant negative Drp1$_{K38A}$ (+Drp1$_{K38A}$), using antibodies against Drp1 or HSP60. (For interpretation of the references to colour in this figure legend, the reader is referred to the web version of this article.)
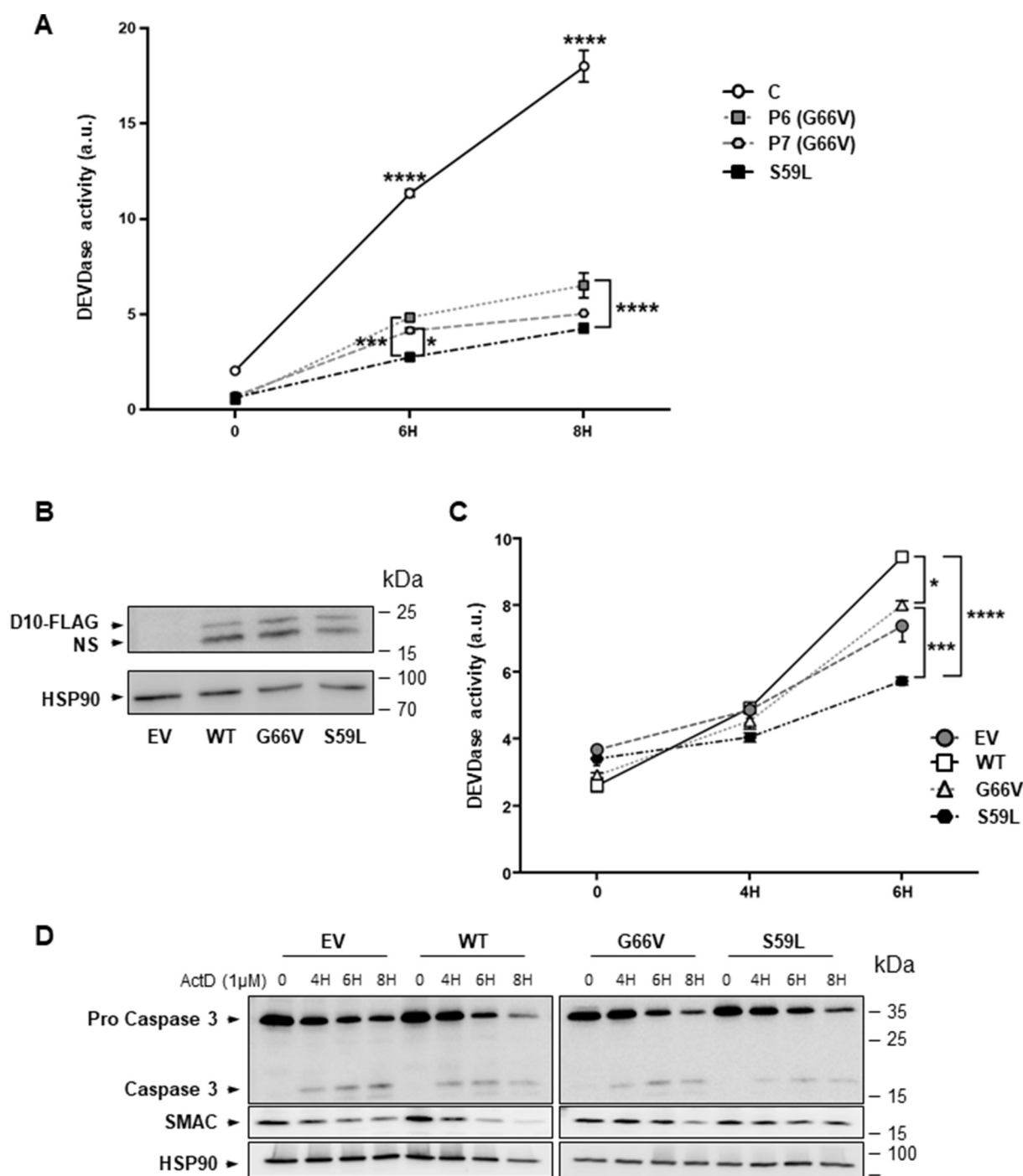
Fig. 6. Inhibition of apoptotic cell death in cells expressing the *CHCHD10^G66V* mutant allele. A. DEVDase activity measured in cell extracts of control, S59L and G66V (P6 and P7) fibroblasts that were treated with 1 μM of staurosporine (STS) for 6 or 8 h. Three independent experiments were performed per condition with two points analysed per experiment. Values are mean ± SD. Differences between the control and patient fibroblasts were analysed by two-way ANOVA: significant (*0.05 > P > 0.01), very significant (***0.005 > P > 0.001) or extremely significant (****P < 0.0001). Absence of significance = non significant. **B–D.** Transfections in HeLa cells were performed with empty vector (EV) or vectors encoding either wild-type CHCHD10-FLAG (WT) or mutant CHCHD10-FLAG (G66V and S59L). **B.** Western blot on HeLa cell extracts using antibodies against FLAG (to detect overexpressed CHCHD10 proteins). HSP90 is used as a loading control. NS: non specific. **C–D.** HeLa cells transiently expressing the WT or mutated forms of CHCHD10-FLAG (G66V or S59L) were treated with 1 μM actinomycin D (ActD) and DEVDase activity was then measured (**C**) from three independent experiments. Differences between the mutated and non-mutated alleles were analysed by two-way ANOVA: significant (*0.05 > P > 0.01), very significant (***0.005 > P > 0.001) or extremely significant (****P<0.0001). **D.** Active caspase 3 and mitochondrial outer membrane permeabilization (by investigating SMAC degradation) were determined by western blot. HSP90 was used as a loading control.

were more severe than that of the R15L mutation (Woo et al., 2017). Because the S59L mutation was found in patients with severe ALS-FTD phenotype whereas the R15L mutation was carried by patients with ALS phenotype only, they suggested that differences observed may reflect

the severity of the phenotypes. Our findings are in agreement with this hypothesis. The p.Gly66Val mutation is responsible for a benign form of lower motor neuron disease and the cellular phenotypes found in S59L and G66V fibroblasts are different. G66V fibroblasts do not display

mitochondrial dysfunction and MICOS assembly defect compared to S59L cells. Both S59L and G66V fibroblasts show comparable mitochondrial accumulation of phosphorylated TDP-43 but the effects on mitochondrial fragmentation and cell death are significantly less pronounced in G66V than in S59L cells.

5. Conclusions and significance

MICOS disassembly has also been described in early-onset fatal mitochondrial encephalopathy with liver disorder (Guarani et al., 2016). In this disease, affected children carried a homozygous loss-of-function mutation in *QIL1* encoding a subunit of MICOS. Patient fibroblasts exhibited MICOS assembly defect with respiratory chain deficiency and abnormal mitochondrial cristae. The rapidly fatal evolution does not make possible to say if these children could have developed a motor neuron disease. Our findings suggest that loss of MICOS complex integrity and mitochondrial dysfunction are likely essential to develop a severe *CHCHD10*-related motor neuron disease whereas accumulation of phosphorylated TDP-43 within mitochondria would not be a criteria of severity. However, these experiments need to be performed in neuron cells to understand the respective role of MICOS complex and TDP-43 in this disease.

Supplementary data to this article can be found online at https://doi.org/10.1016/j.nbd.2018.07.027.

References

Adachi, Y., Itoh, K., Yamada, T., Cerveny, K.L., Suzuki, T.L., Macdonald, P., Frohman, M.A., Ramachandran, R., Iijima, M., Sesaki, H., 2016. Coincident phosphatidic acid interaction restrains Drp1 in mitochondrial division. Mol. Cell 63, 1034–1043. https://doi.org/10.1016/j.molcel.2016.08.013.
Alexander, C., Votruba, M., Pesch, U.E., Thiselton, D.L., Mayer, S., Moore, A., Rodriguez, M., Kellner, U., Leo-Kottler, B., Auburger, G., Bhattacharya, S.S., Wissinger, B., 2000. OPA1, encoding a dynamin-related GTPase, is mutated in autosomal dominant optic atrophy linked to chromosome 3q28. Nat. Genet. 26, 211–215. https://doi.org/10.1038/79944.
Arai, T., Hasegawa, M., Akiyama, H., Ikeda, K., Nonaka, T., Mori, H., Mann, D., Tsuchiya, K., Yoshida, M., Hashizume, Y., Oda, T., 2006. TDP-43 is a component of ubiquitin-positive tau-negative inclusions in frontotemporal lobar degeneration and amyotrophic lateral sclerosis. Biochem. Biophys. Res. Commun. 351, 602–611. https://doi.org/10.1016/j.bbrc.2006.10.093.
Auranen, M., Ylikallio, E., Shcherbii, M., Paetau, A., Kiuru-Enari, S., Toppila, J.P., Tyynismaa, H., 2015. CHCHD10 variant p.(Gly66Val) causes axonal Charcot-Marie-Tooth disease. Neurol. Genet. 1, e1. https://doi.org/10.1212/NXG.0000000000000003.
Ballinger, S.W., Van Houten, B., Conklin, C.A., Jin, G.-F., Godley, B.F., 1999. Hydrogen peroxide causes significant mitochondrial DNA damage in human RPE cells. Exp. Eye Res. 68, 765–772. https://doi.org/10.1006/exer.1998.0661.
Bannwarth, S., Ait-El-Mkadem, S., Chaussenot, A., Genin, E.C., Lacas-Gervais, S., Fragaki, K., Berg-Alonso, L., Kageyama, Y., Serre, V., Moore, D.G., Verschueren, A., Rouzier, C., Le Ber, I., Augé, G., Cochaud, C., Lespinasse, F., N'Guyen, K., de Septenville, A., Brice, A., Yu-Wai-Man, P., Sesaki, H., Pouget, J., Paquis-Flucklinger, V., 2014. A mitochondrial origin for frontotemporal dementia and amyotrophic lateral sclerosis through CHCHD10 involvement. Brain J. Neurol. 137, 2329–2345. https://doi.org/10.1093/brain/awu138.
Buratti, E., Dörk, T., Zuccato, E., Pagani, F., Romano, M., Baralle, F.E., 2001. Nuclear

factor TDP-43 and SR proteins promote in vitro and in vivo CFTR exon 9 skipping. EMBO J. 20, 1774–1784. https://doi.org/10.1093/emboj/20.7.1774.
Chanson, J.-B., Echaniz-Laguna, A., Vogel, T., Mohr, M., Benoilid, A., Kaltenbach, G., Kiesmann, M., 2010. TDP43-positive intraneuronal inclusions in a patient with motor neuron disease and Parkinson's disease. Neurodegener. Dis. 7, 260–264. https://doi.org/10.1159/000273591.
Chaussenot, A., Le Ber, I., Ait-El-Mkadem, S., Camuzat, A., de Septenville, A., Bannwarth, S., Genin, E.C., Serre, V., Augé, G., Brice, A., Pouget, J., Paquis-Flucklinger, V., 2014. Screening of CHCHD10 in a French cohort confirms the involvement of this gene in frontotemporal dementia with amyotrophic lateral sclerosis patients. Neurobiol. Aging 35 https://doi.org/10.1016/j.neurobiolaging.2014.07.022. 2884.e1–4.
Cozzolino, M., Rossi, S., Mirra, A., Carrì, M.T., 2015. Mitochondrial dynamism and the pathogenesis of Amyotrophic Lateral Sclerosis. Front. Cell. Neurosci. 9, 31. https://doi.org/10.3389/fncel.2015.00031.
De Conti, L., Akinyi, M.V., Mendoza-Maldonado, R., Romano, M., Baralle, M., Buratti, E., 2015. TDP-43 affects splicing profiles and isoform production of genes involved in the apoptotic and mitotic cellular pathways. Nucleic Acids Res. 43, 8990–9005. https://doi.org/10.1093/nar/gkv814.
DeJesus-Hernandez, M., Mackenzie, I.R., Boeve, B.F., Boxer, A.L., Baker, M., Rutherford, N.J., Nicholson, A.M., Finch, N.A., Flynn, H., Adamson, J., Kouri, N., Wojtas, A., Sengdy, P., Hsiung, G.-Y.R., Karydas, A., Seeley, W.W., Josephs, K.A., Coppola, G., Geschwind, D.H., Wszolek, Z.K., Feldman, H., Knopman, D.S., Petersen, R.C., Miller, B.L., Dickson, D.W., Boylan, K.B., Graff-Radford, N.R., Rademakers, R., 2011. Expanded GGGGCC hexanucleotide repeat in noncoding region of C9ORF72 causes chromosome 9p-linked FTD and ALS. Neuron 72, 245–256. https://doi.org/10.1016/j.neuron.2011.09.011.
Friedman, J.R., Mourier, A., Yamada, J., McCaffery, J.M., Nunnari, J., 2015. MICOS coordinates with respiratory complexes and lipids to establish mitochondrial inner membrane architecture. eLife 4. https://doi.org/10.7554/eLife.07739.
Genin, E.C., Plutino, M., Bannwarth, S., Villa, E., Cisneros-Barroso, E., Roy, M., Ortega-Vila, B., Fragaki, K., Lespinasse, F., Pinero-Martos, E., Augé, G., Moore, D., Burté, F., Lacas-Gervais, S., Kageyama, Y., Itoh, K., Yu-Wai-Man, P., Sesaki, H., Ricci, J.-E., Vives-Bauza, C., Paquis-Flucklinger, V., 2016. CHCHD10 mutations promote loss of mitochondrial cristae junctions with impaired mitochondrial genome maintenance and inhibition of apoptosis. EMBO Mol. Med. 8, 58–72. https://doi.org/10.15252/emmm.201505496.
Guarani, V., Jardel, C., Chrétien, D., Lombès, A., Bénit, P., Labasse, C., Lacène, E., Bourillon, A., Imbard, A., Benoist, J.-F., Dorboz, I., Gilleron, M., Goetzman, E.S., Gaignard, P., Slama, A., Elmaleh-Bergès, M., Romero, N.B., Rustin, P., Ogier De Baulny, H., Paulo, J.A., Harper, J.W., Schiff, M., 2016. QIL1 mutation causes MICOS disassembly and early onset fatal mitochondrial encephalopathy with liver disease. eLife 5. https://doi.org/10.7554/eLife.17163.
Janssens, J., Van Broeckhoven, C., 2013. Pathological mechanisms underlying TDP-43 driven neurodegeneration in FTLD-ALS spectrum disorders. Hum. Mol. Genet. 22, R77–R87. https://doi.org/10.1093/hmg/ddt349.
Jokela, M.E., Joutsa, J., Udd, B., 2016. Evolving neuromuscular phenotype in a patient with a heterozygous CHCHD10 p.G66V mutation. J. Neurol. 263, 1461–1462. https://doi.org/10.1007/s00415-016-8134-z.
Josephs, K.A., Whitwell, J.L., Tosakulwong, N., Weigand, S.D., Murray, M.E., Liesinger, A.M., Petrucelli, L., Senjem, M.L., Ivnik, R.J., Parisi, J.E., Petersen, R.C., Dickson, D.W., 2015. TAR DNA-binding protein 43 and pathological subtype of Alzheimer's disease impact clinical features. Ann. Neurol. 78, 697–709. https://doi.org/10.1002/ana.24493.
Kabashi, E., Valdmanis, P.N., Dion, P., Spiegelman, D., McConkey, B.J., Vande Velde, C., Bouchard, J.-P., Lacomblez, L., Pochigaeva, K., Salachas, F., Pradat, P.-F., Camu, W., Meininger, V., Dupre, N., Rouleau, G.A., 2008. TARDBP mutations in individuals with sporadic and familial amyotrophic lateral sclerosis. Nat. Genet. 40, 572–574. https://doi.org/10.1038/ng.132.
Kageyama, Y., Zhang, Z., Sesaki, H., 2011. Mitochondrial division: molecular machinery and physiological functions. Curr. Opin. Cell Biol. 23, 427–434. https://doi.org/10.1016/j.ceb.2011.04.009.
Kim, J.-S., Lee, C., Bonifant, C.L., Ressom, H., Waldman, T., 2007. Activation of p53-dependent growth suppression in human cells by mutations in PTEN or PIK3CA. Mol. Cell. Biol. 27, 662–677. https://doi.org/10.1128/MCB.00537-06.
Knott, A.B., Bossy-Wetzel, E., 2008. Impairing the mitochondrial fission and fusion balance: a new mechanism of neurodegeneration. Ann. N. Y. Acad. Sci. 1147, 283–292. https://doi.org/10.1196/annals.1427.030.
Moraes, C.T., DiMauro, S., Zeviani, M., Lombes, A., Shanske, S., Miranda, A.F., Nakase, H., Bonilla, E., Werneck, L.C., Servidei, S., 1989. Mitochondrial DNA deletions in progressive external ophthalmoplegia and Kearns-Sayre syndrome. N. Engl. J. Med. 320, 1293–1299. https://doi.org/10.1056/NEJM198905183202001.
Neumann, M., Sampathu, D.M., Kwong, L.K., Truax, A.C., Micsenyi, M.C., Chou, T.T., Bruce, J., Schuck, T., Grossman, M., Clark, C.M., McCluskey, L.F., Miller, B.L., Masliah, E., Mackenzie, I.R., Feldman, H., Feiden, W., Kretzschmar, H.A., Trojanowski, J.Q., Lee, V.M.-Y., 2006. Ubiquitinated TDP-43 in frontotemporal lobar degeneration and amyotrophic lateral sclerosis. Science 314, 130–133. https://doi.org/10.1126/science.1134108.
Nijtmans, L.G.J., Henderson, N.S., Holt, I.J., 2002. Blue Native electrophoresis to study mitochondrial and other protein complexes. Methods 26, 327–334. https://doi.org/10.1016/S1046-2023(02)00038-5.
Pasanen, P., Myllykangas, L., Pöyhönen, M., Kiuru-Enari, S., Tienari, P.J., Laaksovirta, H., Toppila, J., Ylikallio, E., Tyynismaa, H., Auranen, M., 2016. Intrafamilial clinical variability in individuals carrying the CHCHD10 mutation Gly66Val. Acta Neurol. Scand. 133, 361–366. https://doi.org/10.1111/ane.12470.
Penttilä, S., Jokela, M., Bouquin, H., Saukkonen, A.M., Toivanen, J., Udd, B., 2015. Late

onset spinal motor neuronopathy is caused by mutation in CHCHD10. Ann. Neurol. 77, 163–172. https://doi.org/10.1002/ana.24319.

Penttilä, S., Jokela, M., Saukkonen, A.M., Toivanen, J., Palmio, J., Lähdesmäki, J., Sandell, S., Shcherbii, M., Auranen, M., Ylikallio, E., Tyynismaa, H., Udd, B., 2017. CHCHD10 mutations and motor neuron disease: the distribution in Finnish patients. J. Neurol. Neurosurg. Psychiatry 88, 272–277. https://doi.org/10.1136/jnnp-2016-314154.

Renton, A.E., Majounie, E., Waite, A., Simón-Sánchez, J., Rollinson, S., Gibbs, J.R., Schymick, J.C., Laaksovirta, H., van Swieten, J.C., Myllykangas, L., Kalimo, H., Paetau, A., Abramzon, Y., Remes, A.M., Kaganovich, A., Scholz, S.W., Duckworth, J., Ding, J., Harmer, D.W., Hernandez, D.G., Johnson, J.O., Mok, K., Ryten, M., Trabzuni, D., Guerreiro, R.J., Orrell, R.W., Neal, J., Murray, A., Pearson, J., Jansen, I.E., Sondervan, D., Seelaar, H., Blake, D., Young, K., Halliwell, N., Callister, J.B., Toulson, G., Richardson, A., Gerhard, A., Snowden, J., Mann, D., Neary, D., Nalls, M.A., Peuralinna, T., Jansson, L., Isoviita, V.-M., Kaivorinne, A.-L., Hölttä-Vuori, M., Ikonen, E., Sulkava, R., Benatar, M., Wuu, J., Chiò, A., Restagno, G., Borghero, G., Sabatelli, M., ITALSGEN Consortium, Heckerman, D., Rogaeva, E., Zinman, L., Rothstein, J.D., Sendtner, M., Drepper, C., Eichler, E.E., Alkan, C., Abdullaev, Z., Pack, S.D., Dutra, A., Pak, E., Hardy, J., Singleton, A., Williams, N.M., Heutink, P., Pickering-Brown, S., Morris, H.R., Tienari, P.J., Traynor, B.J., 2011. A hexanucleotide repeat expansion in C9ORF72 is the cause of chromosome 9p21-linked ALS-FTD. Neuron 72, 257–268. https://doi.org/10.1016/j.neuron.2011.09.010.

Robinson, B.H., Petrova-Benedict, R., Buncic, J.R., Wallace, D.C., 1992. Nonviability of cells with oxidative defects in galactose medium: a screening test for affected patient fibroblasts. Biochem. Med. Metab. Biol. 48, 122–126.

Rouzier, C., Bannwarth, S., Chaussenot, A., Chevrollier, A., Verschueren, A., Bonello-Palot, N., Fragaki, K., Cano, A., Pouget, J., Pellissier, J.-F., Procaccio, V., Chabrol, B., Paquis-Flucklinger, V., 2012. The MFN2 gene is responsible for mitochondrial DNA instability and optic atrophy "plus" phenotype. Brain J. Neurol. 135, 23–34. https://doi.org/10.1093/brain/awr323.

Rustin, P., Chretien, D., Bourgeron, T., Gérard, B., Rötig, A., Saudubray, J.M., Munnich, A., 1994. Biochemical and molecular investigations in respiratory chain deficiencies. Clin. Chim. Acta 228, 35–51.

Smirnova, E., Shurland, D.L., Ryazantsev, S.N., van der Bliek, A.M., 1998. A human dynamin-related protein controls the distribution of mitochondria. J. Cell Biol. 143, 351–358.

Sreedharan, J., Blair, I.P., Tripathi, V.B., Hu, X., Vance, C., Rogelj, B., Ackerley, S., Durnall, J.C., Williams, K.L., Buratti, E., Baralle, F., de Belleroche, J., Mitchell, J.D.,

Leigh, P.N., Al-Chalabi, A., Miller, C.C., Nicholson, G., Shaw, C.E., 2008. TDP-43 mutations in familial and sporadic amyotrophic lateral sclerosis. Science 319, 1668–1672. https://doi.org/10.1126/science.1154584.

Vives-Bauza, C., Yang, L., Manfredi, G., 2007. Assay of mitochondrial ATP synthesis in animal cells and tissues. Methods Cell Biol. 80, 155–171. https://doi.org/10.1016/S0091-679X(06)80007-5.

Wang, W., Li, L., Lin, W.-L., Dickson, D.W., Petrucelli, L., Zhang, T., Wang, X., 2013. The ALS disease-associated mutant TDP-43 impairs mitochondrial dynamics and function in motor neurons. Hum. Mol. Genet. 22, 4706–4719. https://doi.org/10.1093/hmg/ddt319.

Wang, W., Wang, L., Lu, J., Siedlak, S.L., Fujioka, H., Liang, J., Jiang, S., Ma, X., Jiang, Z., da Rocha, E.L., Sheng, M., Choi, H., Lerou, P.H., Li, H., Wang, X., 2016. The inhibition of TDP-43 mitochondrial localization blocks its neuronal toxicity. Nat. Med. 22, 869–878. https://doi.org/10.1038/nm.4130.

Wang, W., Arakawa, H., Wang, L., Okolo, O., Siedlak, S.L., Jiang, Y., Gao, J., Xie, F., Petersen, R.B., Wang, X., 2017. Motor-coordinative and cognitive dysfunction caused by mutant TDP-43 could be reversed by inhibiting its mitochondrial localization. Mol. Ther. 25, 127–139. https://doi.org/10.1016/j.ymthe.2016.10.013.

Weishaupt, J.H., Hyman, T., Dikic, I., 2016. Common Molecular Pathways in Amyotrophic Lateral Sclerosis and Frontotemporal Dementia. Trends Mol. Med. 22, 769–783. https://doi.org/10.1016/j.molmed.2016.07.005.

Woo, J.-A.A., Liu, T., Trotter, C., Fang, C.C., De Narvaez, E., LePochat, P., Maslar, D., Bukhari, A., Zhao, X., Deonarine, A., Westerheide, S.D., Kang, D.E., 2017. Loss of function CHCHD10 mutations in cytoplasmic TDP-43 accumulation and synaptic integrity. Nat. Commun. 8, 15558. https://doi.org/10.1038/ncomms15558.

Xu, Y.-F., Gendron, T.F., Zhang, Y.-J., Lin, W.-L., D'Alton, S., Sheng, H., Casey, M.C., Tong, J., Knight, J., Yu, X., Rademakers, R., Boylan, K., Hutton, M., McGowan, E., Dickson, D.W., Lewis, J., Petrucelli, L., 2010. Wild-type human TDP-43 expression causes TDP-43 phosphorylation, mitochondrial aggregation, motor deficits, and early mortality in transgenic mice. J. Neurosci. 30, 10851–10859. https://doi.org/10.1523/JNEUROSCI.1630-10.2010.

Züchner, S., Mersiyanova, I.V., Muglia, M., Bissar-Tadmouri, N., Rochelle, J., Dadali, E.L., Zappia, M., Nelis, E., Patitucci, A., Senderek, J., Parman, Y., Evgrafov, O., Jonghe, P.D., Takahashi, Y., Tsuji, S., Pericak-Vance, M.A., Quattrone, A., Battaloglu, E., Polyakov, A.V., Timmerman, V., Schröder, J.M., Vance, J.M., Battologlu, E., 2004. Mutations in the mitochondrial GTPase mitofusin 2 cause Charcot-Marie-Tooth neuropathy type 2A. Nat. Genet. 36, 449–451. https://doi.org/10.1038/ng1341.